Sixth International Symposium on Turbulence and Shear Flow Phenomena
Seoul, Korea, 22-24 June 2009

# Experimental Investigation of Automobile Sunroof Buffeting Shear Flows

**Seong Ryong Shin and Moo Sang Kim**
Corporate Research & Development Division
Hyundai Motor Company
772-1 Jangduk-Dong, Hwaseong-Si, Gyeonggi-Do, 445-706, Korea
ssdragon@hyundai.com

**Hyungseok Kook**
School of Mechanical and Automotive Engineering
Kookmin University
861-1 Chongnung-dong, Songbuk-gu, Seoul, 136-702, Korea
kook@kookmin.ac.kr

## ABSTRACT

The automobile sunroof buffeting is the tonal noise of a low frequency around 20Hz. It occurs due to the acoustic feedback process between the shear layer detached from the leading edge of sunroof opening and the Helmholtz resonator-like property of a car cabin. In this work, PIV visualization technique is applied to the unsteady flow field around sunroof opening of a SUV in the full-scale automotive wind tunnel in order to find out buffeting mechanism. A phase-marked PIV measurement method, in which image and sound pressure are recorded simultaneously, and a phase-rearrangement post-processing program were developed for capturing noise-related velocity fields without expensive synchronization systems. Through this study, some characteristics of the real-car sunroof shear layers under various deflector conditions were identified and these results can provide insights into the noise reduction mechanism of the tube-type deflector.

## INTRODUCTION

The sunroof buffeting is a low frequency tonal noise generated by acoustic response of an opened vehicle cabin exposed to a grazing unstable shear flow. It is an aeroacoustic noise generated by a periodic convection of large-structured vortices over the opening. Even though the buffeting frequency is sometimes below the lowest limit of the audio frequency, it still causes annoyance, fatigue, and dizziness to passengers due to its high level (Kook *et al*., 2002).

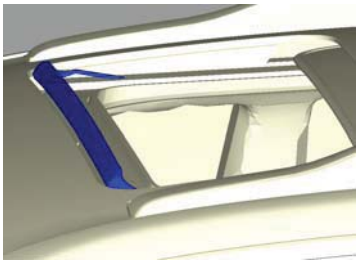

Fig. 1: SUV Sunroof highlighting the deflector.

Sunroof deflectors are usually adopted to reduce the buffeting noise. Deflectors with tube-type cross-sections, one of which is shown in Fig. 1 and 4, are recently widely used, since they are known to be more efficient in reducing the sunroof buffeting. Recently, Shin *et al*. (2006) showed experimentally that buffeting noise level is sensitive to the change in the protrusion but nearly insensitive to the change in gap. The purpose of the present study is to investigate the changes in flow fields caused by changes in deflector protrusion in order to understand the noise suppression mechanism caused by deflectors, eventually.

In the present work, as an experimental approach, a two-frame phase-marked particle image velocimetry (PIV) technique is used. Generally speaking, phase-locked PIV systems are suitable for periodic flow phenomena. But for some laser systems, the repetition rate of pulses is limited depending on the type of the laser, and even fixed in a limited range for an optimal operation. Moreover, the speed of image transmission to the PC memory is limited for relatively low-end PIV systems. For these PIV systems, phase-locked PIV measurements aren't possible from time to time. To overcome the limitations of such systems, a new technique named phase-marked PIV method is used in the present study. Using the phase-marked PIV measurements and a subsequent post-processing procedure that sorts images accordingly to the marked phases, periodic flow of large-structured vortices over a sunroof opening can be obtained when the buffeting noise level is large.

The purpose of the present work is to investigate the effects of the factors, such as the initial shear layer thickness and the free stream flow velocity, on the growth of the shear layer fluctuations and the vortices coalescence process over the sunroof opening.

## PHASE-MARKED PIV MEASUREMENTS

A mid-sized real SUV was used for test and a two-frame PIV measurement system was set up in the test section of the Hyundai Aeroacoustic Wind Tunnel (HAWT). The PIV system used in the experiment is shown in Fig.2. In the system, a dual-pulse Nd-Yag laser was used as a light source. The laser system was optimized to generate dual-pulsed light sheets at a fixed rate between 28 to 32Hz. The camera system has 8-bit 1k x 1k resolution and is capable of capturing double-frame images at a rate of 15Hz. However, the double-framing rate is limited below 5 Hz due to the lower image transmission speed. Moreover, synchronization

with the laser was impossible in the external triggering mode. Therefore, a traditional phase-locked PIV measurement is not possible using this PIV system.

Considering the slow double-framing rate of the image acquisition system, laser repetition rate was fixed at 30 Hz, and double-framed images were taken every seven laser double pulses (i.e., 4.3 Hz). For post-processing purpose, the camera input signal that triggers capturing the first of the double images, and the interior pressure signal measured by a microphone located at the driver's ear position, were simultaneously recorded by a two-channel data acquisition system.

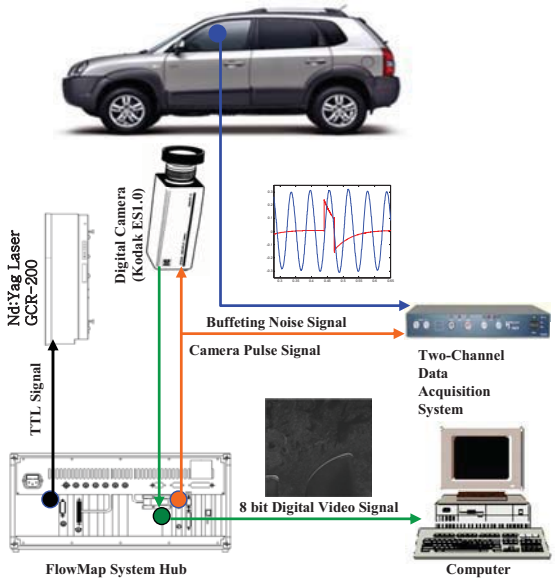


Fig. 2: Experimental system for phase-marked PIV measurement.

Fig. 3: PIV measurement of velocity fields over a sunroof opening in the test section of HAWT.

A nozzle for particle seeding was placed on the slightly left front side of the radiator grille. During the PIV experiments, olive oil was sprayed over the sunroof opening by using seeding equipment. The average size of the olive oil particle is known to be typically 1μm. To avoid the three-dimensional flow effects near the side edges of the sunroof opening, the laser and a mirror were adjusted to form laser sheets on 0L plane of the vehicle (0L plane is an imaginary central plane bisecting a vehicle left and right). The laser and camera systems were established on the left-hand side of the vehicle as shown in Fig.3. At least a distance of 2.5 m was necessary to minimize the vibration of the camera due to the wind in the test section of HAWT during the operation. Because the particle pixel size seen by the camera was too small, a zoom lens was used.

The image area on the measurement plane taken by the camera with the zoom lens was 60 x 60 $mm^2$. Since the area exposed by the camera cannot cover the whole area of interest over the sunroof opening, the measurement plane over the sunroof opening was divided into smaller image areas that can be taken by the camera at a time. As shown in Fig.4, a total of 13 subregions are defined over the sunroof opening space to cover the whole area of interest when the sunroof is fully open.

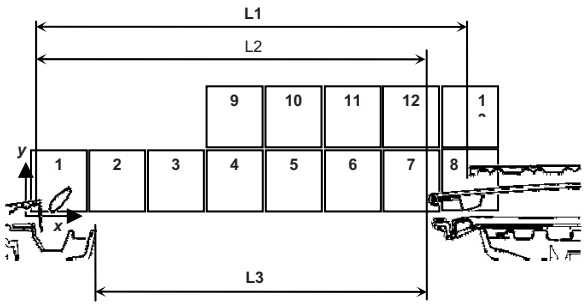


Fig. 4: A sketch of the sunroof opening, subregions for PIV measurements, and the coordinate system.

A total of five different cases of PIV measurements are reported in the present work. For each PIV experiments, the deflector position was varied and summarized in Table 1. The first case named def0 is a baseline test without the deflector. The tube-type deflector used in the experiments was designed to be used at an angle of 44° and can maintain a uniform spacing with the channel of frame-A along the span only when used at that angle. The angle and the gap of the deflector were maintained at 44° and 18mm, respectively, since uniform velocity fields on the planes along the span direction were desired and the buffeting noise level was shown to be insensitive to the changes in the gap variation. The deflector case named def1 is the lowest protrusion case tested, and about 4mm were incrementally increased in protrusion for the rest of the cases. All the PIV experiments reported in the present article were performed with a free stream flow velocity of 50km/h. The frequency and A-weighted sound pressure level of the buffeting noise for each deflector case is shown in Table 1. The use of def3 reduced the buffeting noise by 50 % in energy (3dB). Buffeting noise level was significantly reduced by def4, and the noise level was drifted from 43 to 54dBA. Experimental results show that increase in protrusion generally decreases the buffeting noise level.

A maximum number of 5,000 and at least 2,500 pairs of particle images were taken at one subregion. To obtain 5,000 pairs of particles images at one subregion at a double-framing rate of 4.3Hz, it approximately takes 30 minutes, and 10GB of memory space for images only. Considering the limited experimental time and memory space, particle images were taken in all of subregions defined in Fig.4 only for the cases of def0 (i.e., without deflector) and def4. For the rest of the deflector cases, images were taken in only some of the subregions.

Table 1: Various deflector conditions and buffeting noise levels. The angle and gap in each case were approximately 44° and 18mm, respectively.

| Deflector case name | protrusion (mm) | buffeting noise | |
|---|---|---|---|
| | | (Hz) | (dBA) |
| def0 | without deflector | 16.5 | 65.3 |
| def1 | 15 | 17 | 65.6 |
| def2 | 19 | 17 | 64.6 |
| def3 | 23 | 17 | 62.8 |
| def4 | 26 | 17 | 43-54 |

## DATA PROCESSING PROCEDURE

The particle images were processed to yield instantaneous velocity fields. An interrogation window of 64 x 64 was used with 75% overlapping to yield 60 x 60 resolution velocity vector fields (velocity vectors with approximately 1mm spacing both in the x- and y-directions). To identify the phase of each instantaneous velocity field, the time-captured data containing the interior sound pressure and camera triggering pulses was post-processed. The interior sound signal was first band-pass filtered to yield a pure sinusoid at the buffeting noise frequency, and the timing of each pulse associated with an instantaneous velocity field was compared with the sinusoid to identify the corresponding phase in the buffeting cycle. The whole instantaneous velocity fields were then sorted according to the phase values identified.

To calculate "phase-locked" velocity fields at 32 evenly spaced phases starting from phase 0°, the instantaneous velocity fields falling within a phase-band centered at each phase were averaged. Four different phase-bandwidths were tested to select the best phase-bandwidth in the present work. Provided enough numbers of instantaneous velocity fields within the phase band, the first narrowest phase band would be the best among the phase-bandwidths given in Table 2. The first phase-bandwidth of 11.25° corresponds approximately to 3 % of one cycle of the periodic reference signal, and may yield nearly as accurate phase-locked velocity fields as those obtained by traditional phase-locked PIV methods, since the periodic reference signal itself sometimes drifts a few percents in frequency as in the case of the sunroof buffeting noise. However, the average number of instantaneous velocity fields averaged in each phase band would be only about 156 for the present case (when a total of 5,000 instantaneous velocity fields are taken). The average numbers of the instantaneous velocity fields averaged in each phase band and overlaps between two adjacent phase-windows for wider phase-bandwidths are shown in Table 2.

Table 2: Phase-bandwidths used to obtain phase-locked velocity fields.

| phase-bandwidth | overlap | average number of velocity fields in each window |
|---|---|---|
| 11.25° | 0% | 156 |
| 15° | 25% | 208 |
| 22.5° | 50% | 313 |
| 45° | 75% | 625 |

In the present work, velocity fields obtained by using the wider phase-bandwidths were compared with those obtained by using the narrowest phase-bandwidth in terms of three measures and results are shown in Table 3. Comparisons were made by using the velocity fields obtained in subregions 5 and 6, where velocity fluctuations are apparent as phase changes. The standard deviations of the absolute differences in the phase-locked velocity fields were first investigated. The value $2\sigma$ distributions of the absolute difference in the phase-locked velocities were within 3 % of $U_\infty$ for all cases. It is surprising that phase-locked velocity fields obtained by using the widest phase-bandwidth do not differ much from those obtained by using the narrowest bandwidth.

Table 3: Phase-bandwidths used to obtain phase-locked velocity fields.

| phase-bandwidth | $2\sigma/U_\infty$ | | 95 % of errors within | | |
|---|---|---|---|---|---|
| | $U$ | $V$ | $u_{rms}$ | $v_{rms}$ | $\overline{uv}$ |
| 15° | 1.4 % | 1.0 % | 2.4 % | 0.9 % | 7.0 % |
| 22.5° | 2.0 % | 1.4 % | 2.9 % | 1.3 % | 4.2 % |
| 45° | 2.9 % | 2.7% | 13 % | 5.8 % | 22 % |

Next, from the 32 sequences of the phase-locked velocity fields, root mean square (rms) values of velocity fluctuations were calculated for all cases. The rms of the velocity fluctuation $v_{rms}$ represents the growth of the unstable shear flow at the buffeting frequency. When the phase-bandwidths of 15° and 22.5° were used, 95 % of the rms values of the velocity fluctuations were within 3 % of the rms values evaluated by using the narrowest phase-bandwidth at the corresponding points over the subregions 5 and 6. The rms values obtained by using the four different phase-bandwidths evaluated at a few downstream locations are compared in Fig.5.

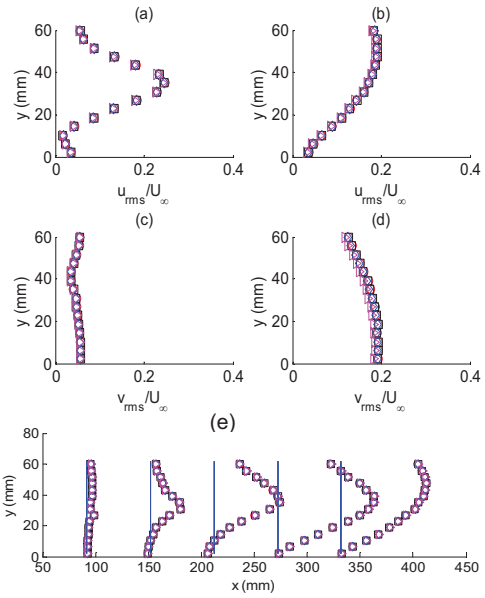


Fig. 5: Comparison of the rms distributions of the buffeting frequency components of velocity fluctuations and phase-averaged Reynolds stresses obtained by four different window sizes given in Table 2; 45° bandwidth (circle);

22.5° bandwidth (square); 15° bandwidth (diamond); 11.25° bandwidth (triangle). (a)$u_{rms}$ at $x$=150 mm; (b)$u_{rms}$ at $x$=330 mm; (c)$v_{rms}$ at $x$=150 mm; (d)$v_{rms}$ at $x$=330 mm; (e)Reynolds stresses evaluated at various downstream stations.

Lastly, the phase-average of the product of velocity fluctuations were compared. The minus of time-average of the product of the velocity fluctuations, $-\overline{uv}$, is called Reynolds stress, and represents the energy transferred to the fluctuations from the mean flow. Therefore, the minus of phase-average of the product of the velocity fluctuations represents the energy transferred to the large-scale vortex structures from the mean flow.(Browand *et al.*, 1987) Compared to other values, the Reynolds stress at the buffeting frequency was a bit sensitive to the choice of a phase-bandwidth as shown in Table 3. For the phase-bandwidths of 45°, the Reynolds stresses were scattered widely from those obtained by using the phase-bandwidth of 11.25°. In the present work, a phase-bandwidth of 22.5° was considered appropriate among the phase-bandwidths investigated, and used to calculate the phase-locked velocity fields hereafter.

## RESULTS AND DISCUSSION

Large-scale vortex structures over the sunroof opening of the test vehicle were successfully identified by using the PIV methods proposed in the present work. In this section, experimental results that show both the large-scale vortex structures and the detailed flow structures near deflectors were presented.

### Large-Scale Structures

In the averaging process to obtain a phase-locked velocity field, small-scale turbulent fluctuations tend to be averaged out, and only periodic components of flow are retrieved. By using the buffeting noise component as a phase reference, large-scale vortex structures associated with the buffeting noise could be obtained. Snapshots of vorticity fields taken at 8 evenly spaced phases beginning from phase 0° are shown in Fig.6. The sequence of the colormaps reveals the evolution of the unstable shear flow as phase changes. The phase 0° represents the instant when the nearly sinusoidal buffeting noise inside the cabin becomes zero and increases.

The shear layer detached near the front-roof edge of the sunroof opening is shown to fluctuate vertically with the amplitude increasing (subregions 1 to 3). Near the subregion 4, the shear layer begins to roll-up to form a discrete vortex at some phase near 45° as shown in Fig. 6(b) and (c). The discrete vortex convects downstream and impinges on the sunroof glass at phase around 225°. It is distorted and convects further downstream over the rear roof. The evolution of the phase-locked vorticity fields obtained for the shear flow over the sunroof opening seems to agree well with experimental results[7,8] observed in small cavities.

The core positions of the discrete vortex convecting downstream were obtained by inspecting the phase-locked velocity fluctuation fields (Fig.7). A discrete vortex structure could be identified from phase 56° (downstream station near 200mm). Until the vortex reaches a downstream station near 350mm, it is shown to convect nearly horizontally. Near the rear edge of the sunroof opening, the vortex convection speed slows down, and accelerates again as the vortex convects over the rear roof. The mean flow velocity in the $x$-direction above the shear layer was 115% of the nominal free stream velocity (i.e., 50km/h) due to the flow acceleration over the windshield glass of the vehicle. The average vortex convection velocity over the sunroof opening estimated from Fig.6 was about 45% of the nominal free stream velocity.

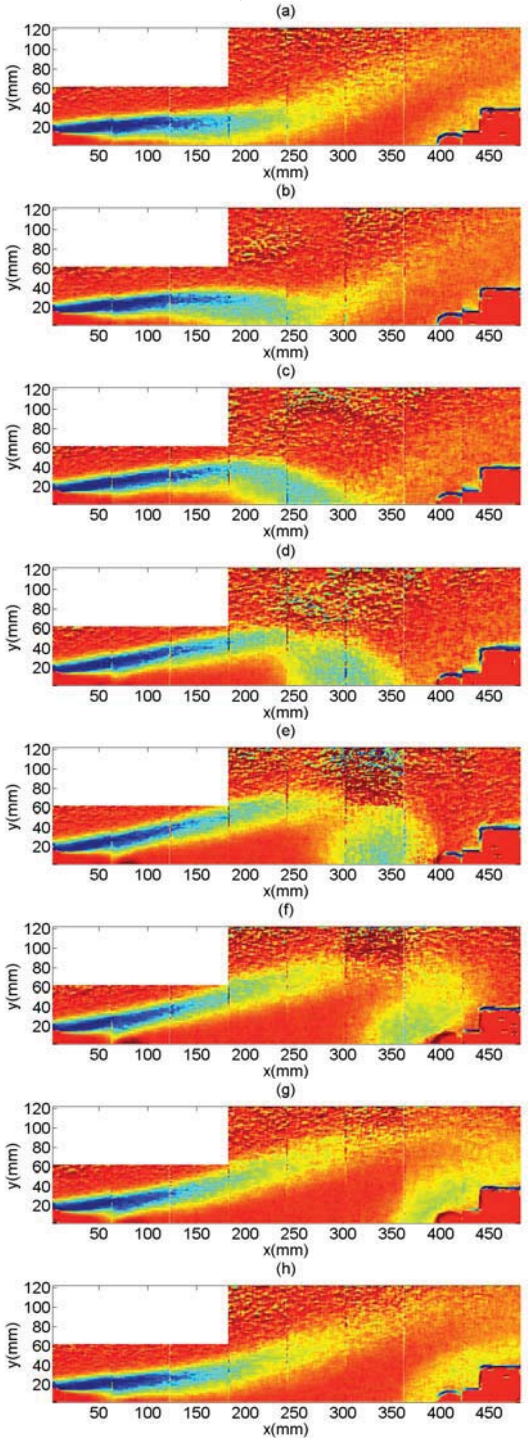


Fig. 6: Colormaps for the vorticity distributions evaluated at buffeting frequency phases of (a) 0°, (b) 45°,

(c) 90°, (d) 135°, (e) 180°, (f) 225°, (g) 270°, and (h) 315°, for the case of def0.

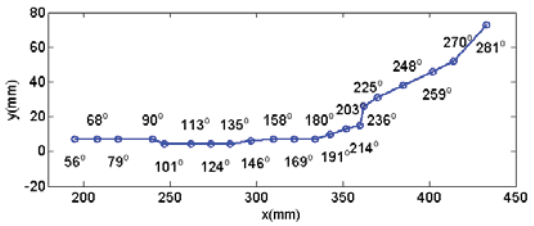


Fig. 7: Convection of the center of a large vortex as phase changes for the case of def0.

In Table 1, the deflector def4 was shown to reduce the buffeting noise level more than 10 dB compared with the case without deflector. To visualize the effects of the deflector on the shear flow over the sunroof opening, colormaps for the root mean square of the velocity fluctuations in the *y*-direction are compared in Fig.8 for the cases of def0 and def4. The mean value meant to be sum of energy in fluctuations at all frequencies was obtained by ensemble-averaging the squares of all the instantaneous velocity fluctuations in the *y*-direction. For the case of def0, the fluctuation energy is shown to grow rapidly as flow convects downstream and has a peak value in subregion 6. For the case of def4, fluctuation energy has a peak value at a station of a few spans downstream of the deflector, but does not grow further in amplitude as flow convects downstream. Besides, it can be observed that the shear layer departs tangentially to the upper surface of the deflector. The shear layer stays higher as it convects downstream due to the increased height and angle of the detachment surface.

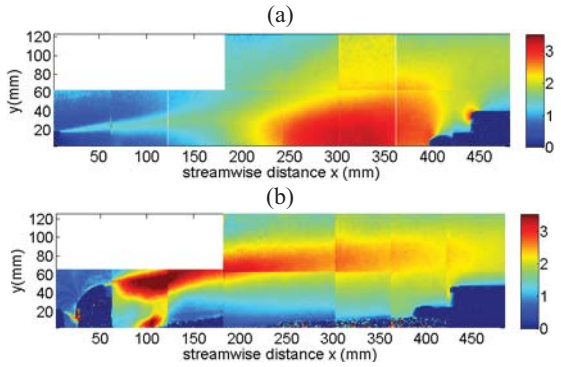


Fig. 8: Root mean square of the velocity fluctuations in the *y*-direction (mean values obtained by ensemble-averaging the squares of all the instantaneous velocity fluctuations. (a) def0, (b) def4

The root mean squares obtained by phase-averaging the squares of the phase-locked velocity fluctuations at the 32 evenly spaced phases are also compared in Fig.9. The phase-averaged rms value represents the fluctuation energy at the buffeting frequency component. As observed in Fig.9(a) for the case without deflector, the buffeting component fluctuation energy occupies the most of the time-averaged energy. This is because the shear flow over the sunroof opening is strongly influenced by the forcing action of the buffeting noise and becomes highly periodic. For the case of def4, the buffeting component of fluctuation energy is shown minimal, and most of the fluctuation energy is at frequencies other than the buffeting frequency.

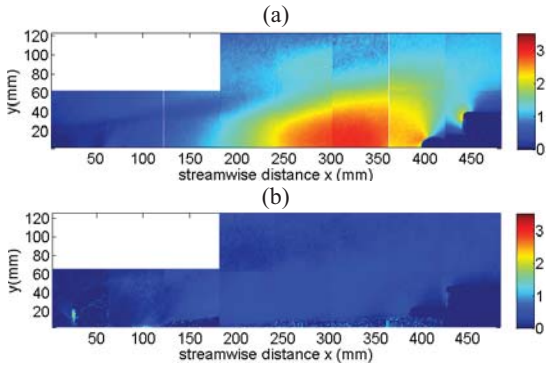


Fig. 9: Root mean square of the velocity fluctuations in the *y*-direction. (a) def0, (b) def4

## Flow Fields near Deflectors

Changes in detailed flow fields near the deflector caused by the changes in the protrusion of the deflector were investigated. The mean velocity vectors for the lowest protrusion and the highest protrusion among the tested protrusions are compared in Fig.10, where the mean velocity components in the *x*-direction are represented as colormaps. One of the main features in the mean velocity fields caused by the higher protrusion is the increased flow under the deflector. Mass flux into the gap between the deflector front and front-roof edge is increased (as shown in subregion 1), and the mass flux is deflected upward approximately at 45° as it exits at the trailing edge of frame-A (as shown in subregion 2). As a result, the shear layer thickness in subregion 3 shown in Fig.10(b) is thicker than that shown in Fig.9(a) due to the increased mass flux under the deflector.

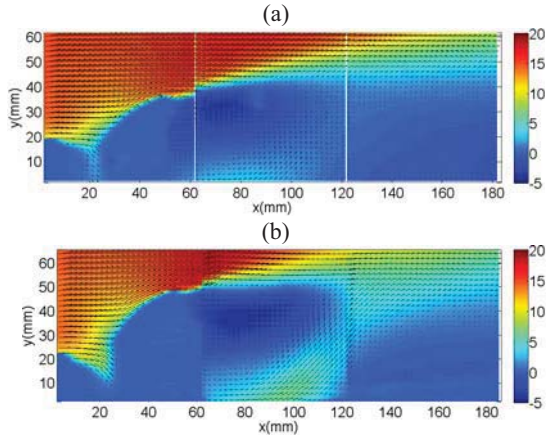


Fig. 10: Velocity vectors (colormaps for the mean velocity in the *x*-direction) in subregions 1 to 3 for the cases of (a) def1 and (b) def4.

The mass flux, momentum fluxes both in the *x*- and *y*-directions, and circulation flux under the deflectors were calculated for the four cases of deflector protrusion, and shown in Fig.11. The net mass flux which is outflux minus influx is supposed to be zero, and calculated as negligibly small except for the case of def2. The negative net

momentum flux in the *x*-direction represents the drag force caused by the deflector and the viscous friction by the frame-A. Overall, the momentum flux in the *y*-direction and the circulation flux are shown increased as the deflector protrusion is increased.

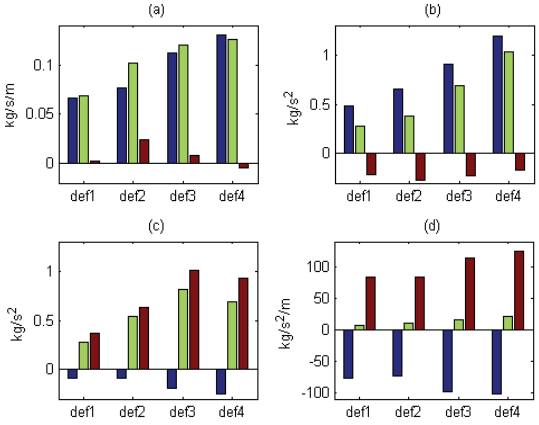


Fig. 11: Balances of flux for the four cases of deflectors; influx (left bar), outflux (central bar), and net outflux (right bar). (a) mass flux; (b) momentum flux in the *x*-direction; (c) momentum flux in the *y*-direction; circulation flux

Many researchers (Voorhees *et al*.(1969), Nelson *et al*.(1981), Sarno *et al*.(1994), Vakili *et at*.(1995), Mandoza *et al*.(1996), and Mongeau *et al*.(1998)) have reported active noise control methods to suppress the noise radiated by cavities exposed to unstable shear flows by injecting secondary flows near the leading edges of the cavity openings. Sarno *et al*.(1994) reported that a steady air flow injected at an angle of 45° effectively suppressed the noise. The comparison of the velocity profiles measured with and without air injection near the leading edge of the cavity openings showed that boundary layer thickness(Mandoza *et al*.(1996)), and the ratio of momentum thickness to the boundary layer thickness(Voorhees *et al*.(1969)) increased with air injection. Many of the researches on noise suppression methods by using mass injection were performed for shallow cavities in a transonic or supersonic range. However, it is believed that the deflected air flow under the deflector in the present work has similar effects with the injected air flows in other researches in reducing the cavity noise.

## CONCLUDING REMARKS

In this study, sunroof buffeting flow fields were investigated through the measurements of flow fields over the sunroof opening of a SUV. Since the PIV system used here is not capable of taking phase-locked velocity fields at the measurement stage, phase-marked PIV measurements were performed and the phase-locked velocity fields were retrieved at a post-processing stage. The new PIV method was shown to yield fairly accurate results with a proper choice of a phase-bandwidth. By using the phase-marked PIV measurement method, the evolution of the large-structured shear flow over the sunroof opening was revealed. Detached shear layer was shown to fluctuate, and then formed a discrete large vortex convecting and impinging on the rear roof edge of the SUV. The average convection velocity of the vortex was calculated to be 45% of the nominal free stream velocity. Flow fields were compared for four different cases of deflector protrusion and a case without deflector.

Installation of a deflector can significantly change the flow field. For a deflector that reduces the buffeting noise by more than 10 dB, it was shown that turbulent fluctuations were initiated due to the deflector, but did not grow in amplitude as they convected downstream. As the deflector protrusion is increased, the amount of flow under the deflector increases in general. The flow exiting from the channel formed by the deflector and a frame-A was shown to increase the thickness of the shear layer near the leading edge of the sunroof opening.of the sunroof opening.

## REFERENCES

Browand F.K., and Ho C.-M., 1987, “Forced, unbounded shear flows”, *Nuclear Physics B*, Vol. 2, pp. 139-158

Kook, H. and Mongeau, L., 2002, “Analysis of the periodic pressure fluctuations induced by flow over a cavity”, *J. Sound and Vibration*, Vol. 251(5), pp. 823-846

Mandoza, J.M. and Ahuja, K.K., 1996, “Cavity Noise Control through Upstream Mass Injection from a Coanda Surface”, *AIAA-96-1767*, pp.1-10

Mongeau, L., Johnson, J.S., Kook, H., and Chang, S., 1998, “Control of vehicle interior pressure oscillations induced by flow over open sunroofs”, *Proceedings of Noise-Con 98*, Ypsilanti, Michigan, April 5-8, pp. 223-228

Nelson, P.A., Halliwell, N.A., and Doak, P.E., 1981, “Fluid dynamics of a flow excited resonance, part I: Experiment”, *J. Sound and Vibration*, Vol. 78(1), pp. 15-38

Sarno, R.L. and Franke, M.E., 1994, "Suppression of Flow Induced Pressure Oscillations in Cavities”, *J. Aircraft*, Vol. 31, pp. 90-96

Shin, S.R., Kim, H.-K., Jung, S.G., and Kook, H., 2006, “New sunroof wind noise reduction strategy using analytical prediction and automatic deflector optimizing system”, *Proceedings of JSAE Annual Congress*

Vakili, A.D., Wolfe, R.C., and Nagle, P.A., 1995, “Active Control of Cavity Aeroacoustics”, *AIAA-95-175*, pp.1199-1206

Voorhees, G.C., and Bertin, J.J., 1969, “Effects of Upstream Mass Injection on the Pressure Field in a Cavity”, *AIAA Journal*, Vol. 7, pp. 747-749